ACS OMEGA

Open Access

http://pubs.acs.org/journal/acsodf

Article

Quantification of the Carbon-Coating Effect on the Interfacial Behavior of Graphite Single Particles

Orynbassar Mukhan, Ji-Su Yun, Hirokazu Munakata, Kiyoshi Kanamura, and Sung-Soo Kim*

Cite This: *ACS Omega* 2024, 9, 4004−4012

Read Online

ACCESS | Metrics & More | Article Recommendations | Supporting Information

ABSTRACT: The effect of carbon coating on the interfacial charge transfer resistance of natural graphite (NG) was investigated by a single-particle measurement. The microscale carbon-coated natural graphite (NG@C) particles were synthesized by the simple wet-chemical mixing method using a phenolic resin as the carbon source. The electrochemical test results of NG@C using the conventional composite electrodes demonstrated desirable rate capability, cycle stability, and enhanced kinetic property. Moreover, the improvements in the composite electrodes were confirmed with the electrochemical parameters (i.e., charge transfer resistance, exchange current density, and solid phase diffusion coefficient) analyzed by a single-particle measurement. The surface carbon coating on the NG particles reduced the interfacial charge transfer resistance (R_{ct}) and increased the exchange current density (i_0). The R_{ct} decreased from 81−101 (NG) to 49−67 Ω cm^2 (NG@C), while i_0 increased from 0.25−0.32 (NG) to 0.38−0.52 mA cm^{-2} (NG@C) after the coating process. The results suggested both electrochemically and quantitatively that the outer uniformly coated surface carbon layer on the graphite particles can improve the solid−liquid interface and other kinetic parameters, therefore enhancing the rate capabilities to obtain the high-power anode materials.

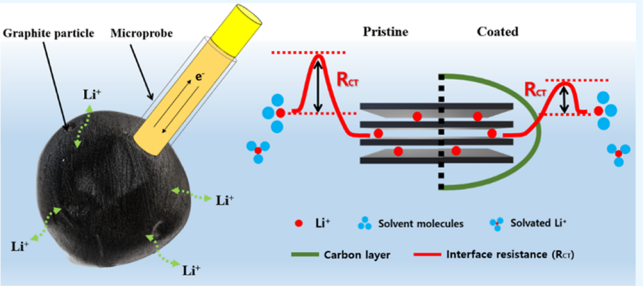

1. INTRODUCTION

Graphite has been widely used as the major market share (>90%) of anode materials since lithium-ion batteries (LIBs) were commercialized. Artificial graphite consumes high energy due to the granulation and high-temperature graphitization processes, and carbon emission is increased.[1,2] Natural graphite (NG) is abundant in the earth's crust with excellent crystal arrangement, which meets the low-carbon environmental protection requirements with the simple purification process.[3,4] However, natural graphite particles suffer the slow intercalation of Li^+ and reduced ion transfer rate because of the inappropriate orientations of the graphite layers. Moreover, due to the low Li^+ diffusion kinetics of natural graphite during fast charging and discharging, a severe amount of Li^+ electroplates at the outer edge of the carbon layer form the lithium dendrites which will make the safety issue of the battery.[5−7] Consequently, the slow kinetics of Li^+ at the interface of natural graphite is one of the key factors that should be considered to obtain a high current performance.

To tackle the issue of low mass transfer of a graphite anode material, several approaches such as coatings, etching,[8,9] doping,[10] expansion,[11] and other methods have been applied to improve Li^+ transportations. Among the various methods, uniform and ultrathin carbon coating on active materials' surfaces is extremely effective in enhancing the electrochemical properties. Initially, the outer carbon-coated layer has effectively increased the intrinsic conductivity of graphite, which promotes fast ionic conduction, resulting in desirable improvement in the rate performance of the anode materials.[12,13] Moreover, the uniform outer carbon layer can avoid direct contact from electrolytes to active material particles by forming a stable solid electrolyte interphase (SEI) layer due to its admirable chemical and electrochemical stabilities of carbon.[14,15] For commercial purposes, the carbonization yield of carbon precursors is one of the crucial factors for low-cost carbon production. The carbon yield of phenolic resin sources is higher compared to the saccharides with a carbon yield of less than 10%.[16] Previous reports also showed improvements in the electrochemical performance of materials such as Si, SiO_x, etc., after the wet carbon-coating process with a phenolic resin as a carbon source.[17,18]

Conventionally, the composite electrodes in the cells for electrochemical characteristics contain a binder, conductive material, and active materials that strongly influence the electrochemical performance of the active material. Moreover, the electrochemical characteristics of the composite electrode

Received: November 2, 2023
Accepted: November 28, 2023
Published: January 8, 2024

are influenced by the structure such as thickness, porosity, tortuosity, and the preparation procedure.[19−21] Thus, these parameters can affect the transport limitations leading to the reduction of the capacity at the high current rates. Therefore, it is difficult to detect the true intrinsic properties of the materials. Single active particle measurements by a microelectrode technique allow for the characterization of the charging and discharging process including intrinsic electrochemical properties such as charge transport resistance, exchange current density, and diffusion coefficient at the one (single) particle levels without the influence of conductive materials, binders, and electrode preparation. Additionally, such measurements can effectively circumvent influential factors affecting composite electrodes, including current density distribution, the nonuniformity of composite electrodes, and coverage of active material by binders.[22] Kanamura et al. reported single-particle measurements on graphite (mesocarbon microbeads, graphite foams, soft carbon) determining the kinetic properties.[23−25] However, these reports performed single-material evaluations, and there are no reports with comparative studies that can characterize the influence of the coating of amorphous carbon on graphite particles.

In the current contribution, we synthesized an ultrathin amorphous carbon coating on graphite as a model to boost the kinetic properties. The natural graphite was coated with the phenolic resin through the traditional wet-chemical mixing method, which was further transformed into an amorphous carbon layer (NG@C) by thermal treating at 1000 °C under an Ar atmosphere. The coated amorphous carbon on graphite considerably improves the rate performance and kinetics of graphite in a working battery cell. The single-particle measurement was carried out to study the effect of coated carbon on the interfacial behavior of graphite.

2. EXPERIMENTAL SECTION

2.1. Material Synthesis. All of the chemicals are used without any further purification as it is provided. An acetone-soluble 2 g of phenolic resin was dissolved in 30 mL of acetone in advance. After that, 3 g of natural graphite (BTR, China) was added to the suspension. The mixture was continuously stirred for 5 h at room temperature. Subsequently, acetone was eliminated from the suspension by using an ultrasonication process. After that, the self-polymerized phenolic resin on natural graphite was collected and dried by using a vacuum rotary evaporator at 110 °C for 2 h and finally calcinated under an Ar atmosphere at 1000 °C for 1 h, at a heating rate of 3 °C/min.

2.2. Structure Characterizations. The X-ray diffraction (XRD) patterns of samples were performed using a PANalytical X'Pert PRO with a Cu Kα radiation source in the range of 10−90° of diffraction angle. Raman spectra were measured by using a LabRam HR-800 spectrometer with a 514 nm excitation laser. Thermogravimetric analysis (TGA, PerkinElmer TGA 8000) was carried out under nitrogen flowing with a heating rate of 5 °C min^{-1}. The morphological analysis of graphite powders was characterized by scanning electron microscopy (SEM) and transmission electron microscopy (Cs-STEM, JEM-ARM200F, JEOL, Japan) with an acceleration voltage of 200 kV. The specific surface areas and porosity of graphite particles were analyzed by Brunauer−Emmett−Teller (BET) and Barrett−Joyner−Halenda (BJH) methods of the nitrogen (N_2) adsorption−desorption isotherms. The surface chemistry of particles was analyzed through X-ray photoelectron spectroscopy (XPS, Thermo Fisher Scientific).

2.3. Electrochemical Measurements. For the formation of NG and NG@C electrodes, the slurry was prepared by mixing active materials, carboxymethyl cellulose (CMC), and styrenebutadiene rubber as binders at a mass ratio of 95:2.5:2.5, in deionized water (DI). The obtained slurry was cast onto the Cu current collector by using a doctor blade method and dried at 110 °C for 5 h. The mass loading and electrode densities of electrodes were ∼5.0 mg cm^{-2} and ∼1.6 g cm^{-3}, respectively. Subsequently, the electrodes were transferred into a dry glovebox filled with high-purity argon gas to make the cells. Electrochemical measurements were tested in a half-cell configuration (CR2016) using lithium metal as the counter electrode/reference electrode. The half-cells were activated with 1 M $LiPF_6$ in EC/EMC (3:7 in vol %, +5% FEC) electrolyte. The cycling and rate performances at 0.2 0.5 1, 2, and 5C (1C = 372 mA g^{-1}) were tested using a battery cycler (ADBT-5-1-36-S, Espec, Japan) at room temperature in a voltage range of 0.005−1.5 V (vs Li/Li^+) with the initial two formation cycles at 0.1C. The galvanostatic intermittent titration technique (GITT) measurement was performed using a series of pulsed currents at 0.1C imposed on the cell for 600 s, followed by 3600 s of rest to reach the quasi-equilibrium state. Electrochemical impedance (EIS) was evaluated with a frequency range of 10^6−10^2 Hz with an AC amplitude of 10 mV (Ivium).

2.4. Single-Particle Measurements. The graphite active anode particles were evaluated by single-particle measurements. Detailed information about single-particle equipment and the procedure was reported in the previous studies.[24,26] A copper-coated gold wire (diameter: ∼17 μm) surrounded by glass capillary was used in the single-particle system. The anode particles were spread on a glass filter paper, and the microprobe interlocked to the micromanipulator (Micro-Support Quick Pro) was connected with the target particle using the CCD camera (Hirox Inc.). A lithium metal foil was used as a counter electrode, and a mixed solvent of ethylene carbonate (EC) and propylene carbonate (PC) (1:1 in volume) containing 1 mol dm^{-3} lithium perchlorate ($LiClO_4$) (Dongwha electrolyte) was used as an electrolyte solution. Charge and discharge tests on the single particle were carried out using a galvanostat (IviumState model, Ivium) in the potential range of 0.005−1.5 V vs Li/Li^+. The initial three cycles were charged and discharged at 1 nA in the CC mode. After this, the charging current was maintained at 1 nA to complete charging. However, during the discharging process, the positive and negative pulsed currents were alternatively applied at a certain depth of discharge (DOD) states. The pulse currents were applied for 5 s, and the peak potentials were measured. The positive and negative currents were repeated up to 1−60 nA. The applied pulse currents and potential peak responses were used to draw the Tafel plots to estimate the charge transfer resistance (R_{ct}). Moreover, the discharge rate properties were measured by controlling the charge current at a constant 1 nA and discharge currents from 1 to 200 nA during subsequent cycles. All of the single-particle measurements were performed in an Ar gas-filled glovebox at room temperature (293 K).

3. RESULTS AND DISCUSSION

3.1. Physical Characterization of the Materials. Low-magnification SEM images of materials in Figure 1a,d indicate

https://doi.org/10.1021/acsomega.3c08681
ACS Omega 2024, 9, 4004−4012

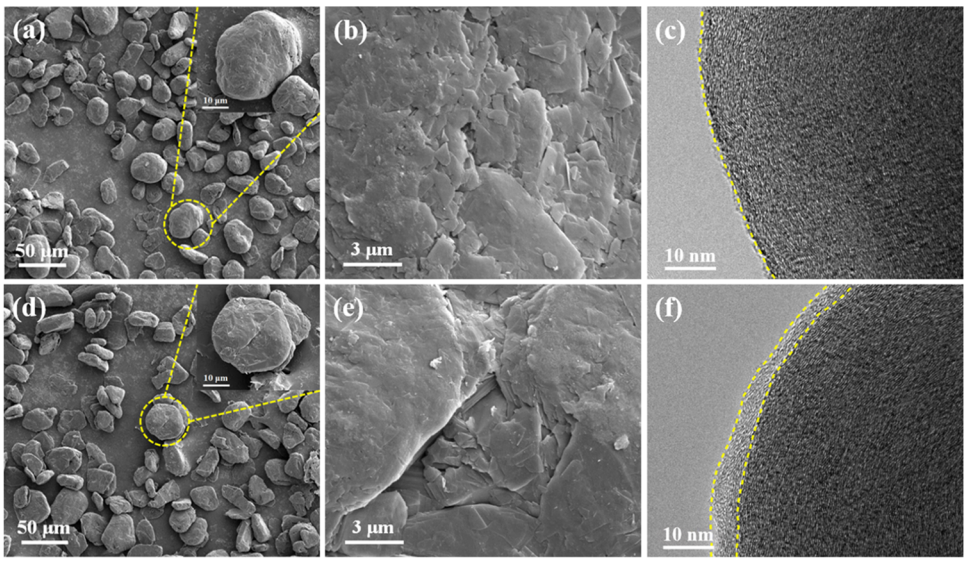

Figure 1. (a, d) Low-magnification and (b,e) high-magnification SEM images and (c, f) TEM images of NG (a−c) and NG@C (d−f). The yellow dashed lines in panel (f) show the outer-coated amorphous carbon layer (~4−5 nm).

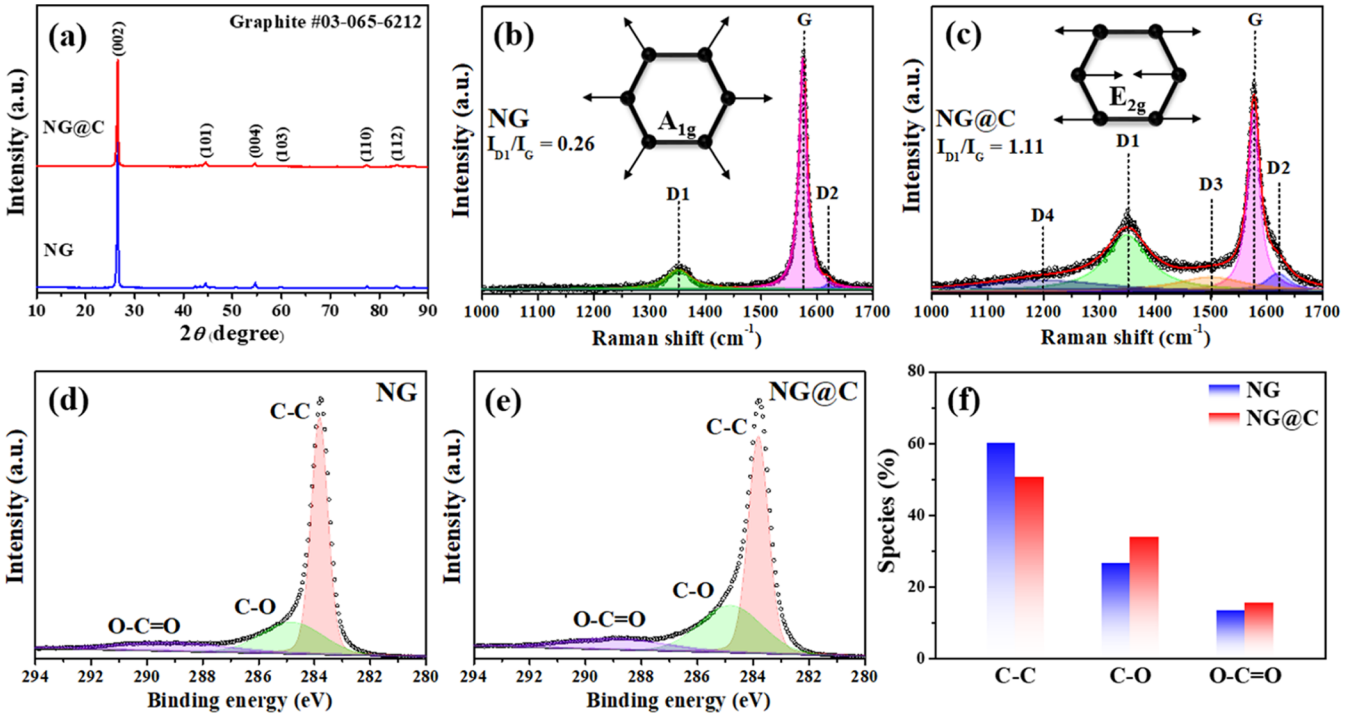

Figure 2. (a) XRD results, Raman results of NG (b) and NG@C (c), and XPS spectra of C 1s (d) NG and (e) NG@C with corresponding species ratios (f).

that samples exhibit spherical potato-like morphology corresponding to the natural graphite which is formed during the spheroidization process of raw flake graphite. High-magnification SEM images in Figure 1b,e show obvious graphite flakes for NG; however, for NG@C, graphite flakes disappeared due to the coated amorphous carbon layer on the surface of natural graphite. The high-resolution TEM images of NG and NG@C as shown in Figure 1c,f reveal a uniform amorphous-like carbon-coating layer on NG. The thickness of the coated carbon layer was observed around 4−5 nm. Such an amorphous-like carbon layer (~4−5 nm) is effective to improve electrochemical performances such as rate retention, cycling stability, kinetics, and other properties of lithium-ion battery graphite anode materials.[27]

The TGA result of NG@C confirms the presence of the amorphous-like carbon with a carbon content of 4.5% (Figure S1). The diffraction patterns in Figure 2a show the diffraction peaks of both the NG and the NG@C samples. The observed peak locations suggest a hexagonal structure with the P63/mmc space group (PDF 03-065-6212). The positions of (002) peaks are identical, but the intensity is lower for NG@C, resulting from an amorphous outer carbon-coating layer. In the Raman spectra of the NG material (Figure 2b,c), typical three peaks appeared at ~1350, 1620, and ~1580 cm^{-2} related to

https://doi.org/10.1021/acsomega.3c08681
ACS Omega 2024, 9, 4004−4012

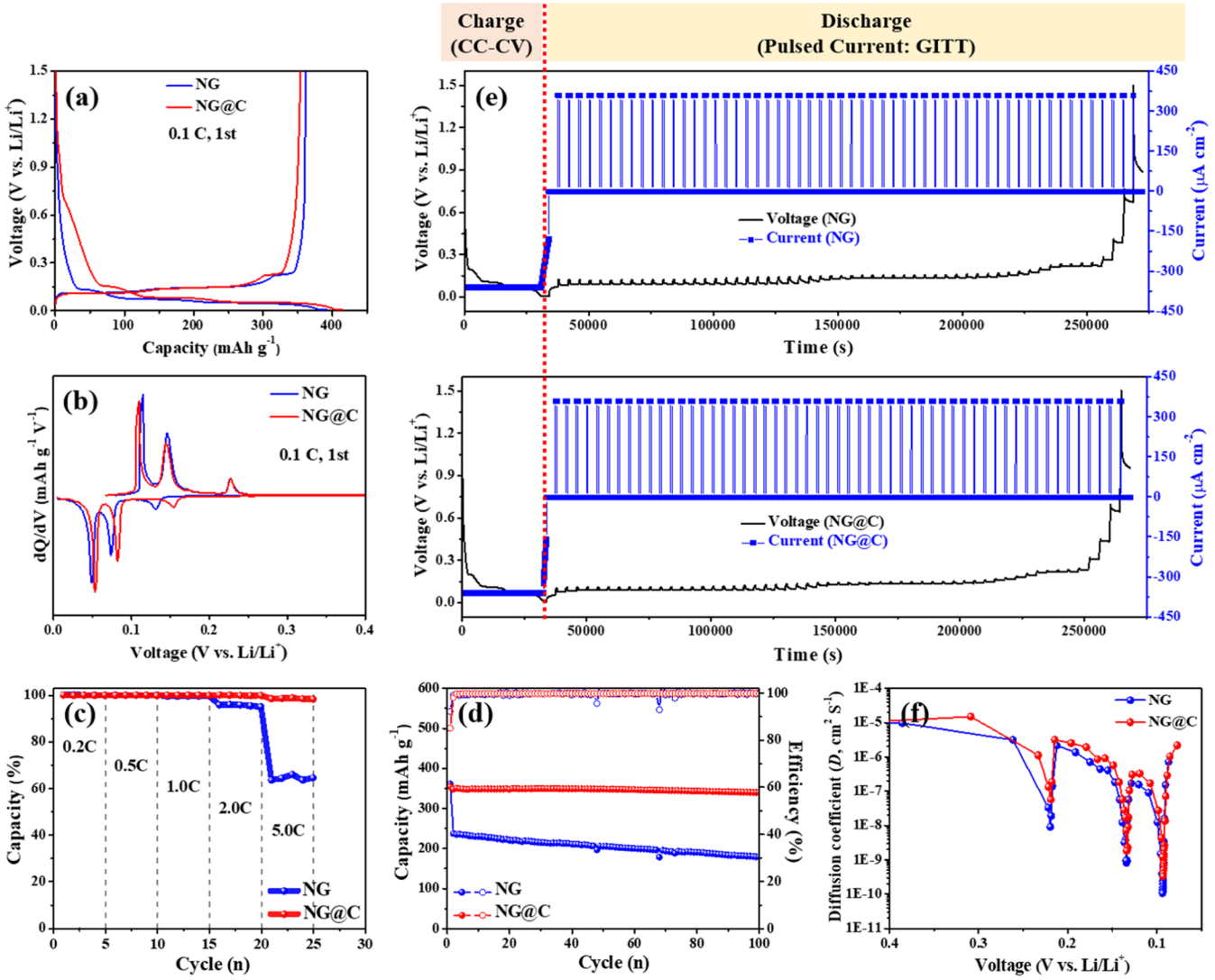

Figure 3. Electrochemical performances of NG and NG@C in half-cells. (a) Charge−discharge curves and corresponding differential plots (b) at 0.1C (1C = 360 mA g^{-1}) for the voltage range of 0.005−1.5 V. (c) Rate performances and (d) cycling performance at 5C. (e) GITT curves and corresponding (f) diffusion coefficient results of NG and NG@C samples.

the weak disorder-induced (D1 and D2) and very strong graphitic (G) bands, respectively. The I_{D1}/I_G value was 0.26. However, in the carbon-coated graphite (NG@C), the D band is broadened and the intensity of the G band is reduced, resulting from the amorphous external coated carbon layer on the surface of NG particles. Accordingly, the broad peak is deconvoluted into several D bands containing D1, D2, D3, and D4. The D1 (∼1350 cm^{-2}) and D2 (∼1620 cm^{-2}) bands come with symmetries of A_{1g} and E_{2g} from graphitic lattice vibration modes. Among them, the D3 band appearing at ∼1500 cm^{-2} and the shoulder at ∼1200 cm^{-2}, expressed as the D4 band, correspond to the amorphous form of carbon and polyene-like structure carbon, respectively. The G band at ∼1580 cm^{-2} corresponds to ideal carbon atoms in the graphite sheets.[28] The I_{D1}/I_G ratio value of NG@C was 1.11, demonstrating defects and disorders of the coated carbon layer on NG, analogous to the XRD results. The Raman results are summarized in Table S1.

Figure S2 shows the X-ray photoelectron spectroscopy survey results of NG and NG@C. From the analysis, it is clearly seen that the carbon species decrease while increasing the oxygen content element. The XPS of C 1s was carried out to characterize the carbon valence states of the graphite samples (Figure 2d−f). The graphite compounds exhibit the typical C−C (∼283.8 eV) and oxygen-containing functional groups of C−O (∼284.8 eV) and C═O (∼289.6 eV) species in the C 1s spectra.[29] After the coating of carbon, smaller C−C content and higher C−O and C═O species can be observed for NG@C compared to the NG. Moreover, the XPS of the O 1s spectra (Figure S3a,b) confirm the presence of a larger amount of C═O functional groups in the NG@C sample (27.6%) than in NG. Overall, the surface of NG@C has an amorphous-like nature, thin, and relatively rich-oxygen carbon layer.

The Brunauer−Emmett−Teller (BET) adsorption/desorption isotherms and pore size distributions of NG and NG@C are shown in Figure S4a,b. The macropore/mesopore/micropore properties determine the shape of the N_2 adsorption/desorption isotherms. According to UIPAC classifications, both graphite specimens exhibited typical type-II isotherms with H3-type hysteretic loops and sharp capillary condensation, corresponding to the meso- and

https://doi.org/10.1021/acsomega.3c08681
ACS Omega 2024, 9, 4004−4012

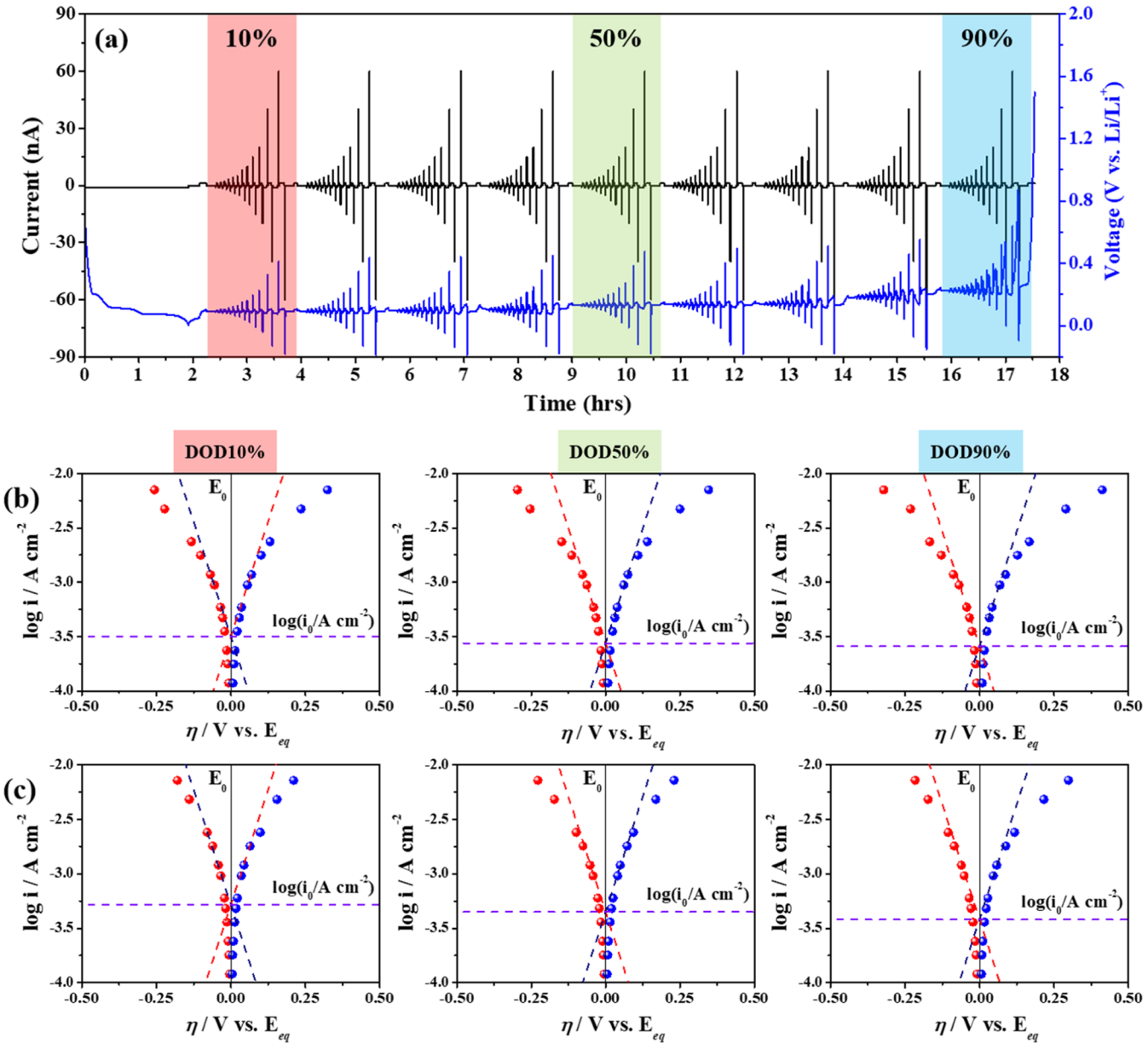

Figure 4. Single-particle measurement of the NG and NG@C particles. (a) Pulse polarization process and Tafel plots at DOD 10%, DOD 50%, and DOD 90% of (b) NG and (c) NG@C single particles.

microporous structure.[30] The BET specific surface areas of NG and NG@C were found to be 4.27 and 47.67 $m^2\ g^{-1}$, respectively. The sharp increase in surface area after carbon coating can be due to the large specific surface area and microporous nature of heat-treated phenolic resin materials.[16,31] The highest surface area facilitates a large amount of Li^+ ions, but it can also increase irreversibility. The pore volumes of NG and NG@C are 0.029 and 0.012 cm^3/g, respectively, whereas pore sizes are 23.2 and 4.32 nm, respectively.

3.2. Electrochemical Characteristics of the NG and NG@C Anodes. The half-cells (2016-type) were assembled to characterize the electrochemical properties of the graphite anodes. Figure 3a shows the charge−discharge curves at 0.1C with initial reversible specific capacities of 361 and 354 mAh g^{-1} for NG and NG@C electrodes with respective initial CE of 92 and 85%. The significantly higher irreversible capacity of NG@C compared with NG is caused by its higher content of oxygen-functional group species and large surface area. Differential curves (d*Q*/d*V*, Figure 3b) reveal that NG and NG@C have multistep lithium−graphite intercalation processes. The smaller voltage polarization between the oxidation and reduction peaks of NG@C suggests better kinetics compared to the NG electrode.[32] Figures 3c and S5a,b demonstrate the rate capability of graphite electrodes at various current densities from 720 (0.2C) to 1800 mA g^{-1} (5C). When the current densities increased, the specific capacity of NG decreased by a larger amount than that of carbon-coated graphite (NG@C). The NG@C electrode showed the fast discharging and charging capability of the graphite anode material. Even at a high current rate of 1800 mA g^{-1} (5C), carbon-coated graphite demonstrated a reversible specific capacity of 348 mAh g^{-1}, corresponding to 98.2% of the capacity obtained at a current density of 720 mA g^{-1} (0.2C). In the case of the pristine natural graphite electrode, it showed a specific capacity of only 230 mAh g^{-1}

https://doi.org/10.1021/acsomega.3c08681
ACS Omega 2024, 9, 4004−4012

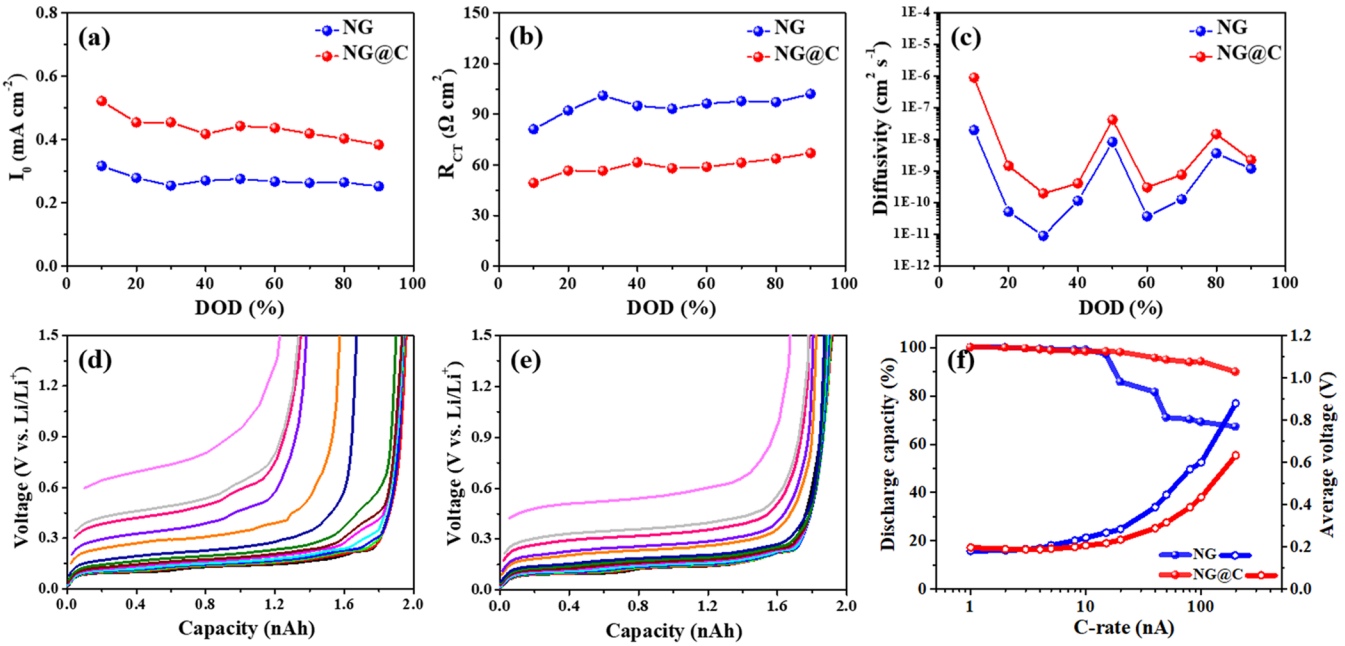

Figure 5. (a) Exchange current densities, (b) charge transfer resistances, and (c) diffusivity results of NG and NG@C single particles obtained from the Tafel plots. Voltage profiles of (d) NG and (e) NG@C single particles at the current range of 1−200 nA and (f) their discharge capacity retention.

(64% of the capacity retention at a current density of 720 mA g^{-1}). Furthermore, the long-term cyclability of graphite electrodes was assessed at 5C after the initial formation cycle at 0.1C (Figure 3d). When the cycling test reaches 100 cycles, the carbon-coated graphite (NG@C) exhibits the highest specific capacity of 340 mAh g^{-1} without noticeable degradation, while the NG electrode delivers only 179 mAh g^{-1} specific capacity with the retention of 96 and 50%, respectively, corresponding to the initial formation cycle capacity. The GITT was carried out to precisely record the Li^+ diffusion in solid graphite electrodes as shown in Figure 3e. Figure 3f shows the results of the Li^+ diffusion behavior of NG and NG@C during the deintercalation process. Both electrodes show a similar trend with a sharply decreasing diffusivity, corresponding to the phase transitions observed in the dQ/dV plot. The NG@C exhibits a significantly improved diffusivity with an average Li^+ diffusion coefficient of 1×10^{-6} cm^2 s^{-1}, while the NG electrode demonstrates an average number of 6.4 $\times 10^{-7}$ cm^2 s^{-1}. The EIS analysis was characterized on the NG and NG@C electrodes. The equivalent circuit can interpret the resistances corresponding to the electrolyte (R_s), SEI (R_{SEI}), charge transfer (R_{ct}), and solid electrode diffusion process.[33] Figure S5c,d illustrates the Nyquist plots of pristine and carbon-coated graphite electrodes after the 2nd and 100th cycles. In the Nyquist plot, after the second cycle, one semicircle was observed in both NG and NG@C electrodes. However, as shown in the inset of Figure S5c,d, the carbon-coated electrode exhibits smaller resistances, especially R_s and R_{ct}, implying the formation of a stable SEI layer compared to the pristine graphite electrode. In general, the resistances of NG and NG@C are summarized in Figure S5e after the 2nd and 100th cycles.

The amplified views of the XRD patterns (25.5−27.5°) in Figure S6 and Table S2 reveal that both NG and NG@C exhibit the presence of (002) peak positions after 100 cycles. The (002) peak of the NG sample shifts to lower diffraction angles and becomes narrower after 100 cycles suggesting the presence of residual lithium in the structure due to the incompleteness of Li ion deintercalation and wider layer space.[34] Notably, the I_{D1}/I_G ratio of the NG anode increases remarkably after galvanostatic cycling, while the NG@C almost does not change, suggesting a stable surface after 100 cycles (Figure S7a−c). The obtained composite electrode results suggest that an amorphous-like carbon layer coated on the graphite can successfully improve the kinetics.

3.3. Single-Particle Measurements. The single-particle measurement was used to investigate the effect of the coated carbon layer on the interfacial behavior of graphite. After the initial three cycles, the graphite particles were fully charged and divided into certain DOD states (every 10%). To estimate the DOD-dependent kinetics of graphite particles, different amplitudes of positive and negative pulse currents were applied, and we measured the potential peak responses. Figure 4a demonstrates the results of a pulse current measurement of the graphite particle.

The correlations of the applied pulse currents and potential peak responses were used to estimate the exchange current densities and interfacial charge transfer resistance; we drew Tafel plots from each DOD of 10%.[35] Figure 4b,c demonstrates the Tafel plots of NG and NG@C particles at DOD 10, 50, and 90%. A larger potential difference (from OCV) was observed for the NG compared to the NG@C. An exchange current density (i_0) was estimated by fitting with a straight line (∼Tafel line) of eqs 1 and 2. The Tafel equations are expressed as follows:[36]

$$\log i_c = \log i_0 + \frac{(1-\alpha)F}{2.303RT}\eta \quad (1)$$

$$\log i_a = \log i_0 + \frac{\alpha F}{2.303RT}\eta \quad (2)$$

Here, i_c and i_a are the applied current densities normalized by the surface area of the particle (assumed spherical, 17 μm), i_0 is

https://doi.org/10.1021/acsomega.3c08681
ACS Omega 2024, 9, 4004−4012

the exchange current density, α is the transference number (assumed to be 0.5) for the cathodic and anodic reactions, F is the Faraday constant, T is the absolute temperature, R is the gas constant, and η ($=E_{eq} - E$) is the overpotential for the cathodic and anodic reactions. Further, the exchange current density and charge transfer resistance at the interface can be correlated and calculated as follows (eq 3):[36]

$$R_{ct} = \frac{RT}{Fi_0} \tag{3}$$

where R_{ct} is the charge transfer resistance.

The calculated exchange current densities were in the range of 0.25−0.32 mA cm^{-2} for the NG, while for NG@C, it demonstrated significantly improved values of 0.38−0.52 mA cm^{-2} during the discharging process. Accordingly, the NG@C particle showed variations of the charge transfer resistance in the range of 49−67 Ω cm^2 which is lower than the pristine NG particle (81−101 Ω cm^2) as shown in Figure 5a,b. The obtained values are considerable with previously reported AC impedance measurements of carbon.[37,38] Our findings have been compared with previously reported R_{ct} results of carbonaceous materials obtained through a single-particle measurement (Table 1). The Li^+ ion diffusion coefficients for the NG and NG@C particles were calculated using Fick's second law from the Tafel plots. Figure 5c depicts the diffusivity of the Li^+ inside the bulk structure, and NG@C exhibits one-order higher diffusivity than the NG sample. Moreover, the rate properties were carried out in the current range of 1−200 nA corresponding to 0.5−100C of current rates as given in Figure 5d−f. The NG@C particle showed ∼90% of capacity retention at 100C, while the NG particle exhibited ∼67% of capacity retention. The improvement of the NG@C particle displays considerably similar behavior to the composite electrode results. Overall, the uniform carbon layer on graphite with the proper structure can significantly enhance the electrochemical performances, kinetics, and interfacial properties of graphite.

Table 1. R_{ct} Results of the Reported Carbonaceous Anode Materials Measured by Single-Particle Techniques

materials	methods	R_{ct} (Ω cm^2)	references
mesocarbon microbeads (MCMB)	overpotential polarization	20−50	Dokko et al.[23]
graphite foam	overpotential polarization	70−120	Lim et al.[24]
soft carbon	overpotential polarization	45−85	Chae et al.[25]
graphitized carbon (MCMB)	AC EIS	27−75	Umeda et al.[37]
disordered carbon (MCMB)	AC EIS	12−79	Dokko et al.[38]
graphite (NG)	pulse polarization	81−102	this work
carbon-coated graphite (NG@C)		49−67	

According to the single-particle measurement and composite electrode results, it was concluded that an amorphous-like layer on graphite considerably reduces the interfacial charge transfer resistance, and the exchange current density increases with regard to pristine graphite. In particular, the rate of Li^+ diffusion of graphite layers at the basal planes is lower compared to that at the edge planes, indicating faster Li^+ intercalation from the edge sides of graphite sheets. However, edge planes suffer from exfoliation and decomposition of the electrolyte rather than basal planes. After coating graphite with an amorphous-like carbon layer, it can provide active sites for easier Li^+ transportation at the basal plane and prevent edge planes from the electrolyte.[39] The coated phenolic resin-based carbon affords the rapid delivery of Li^+ to the edge sides of the graphite layer, resulting in enhanced kinetics (Figure 6). Thus, the coating of graphite with an amorphous-like carbon layer is favorable for improving the high-rate performance of graphite in LIBs.

4. CONCLUSIONS

The microscale NG particles were coated with phenolic resin-based carbon by a simple wet-chemical mixing method. The XRD, Raman, and TEM results suggest coating of a thin (∼4−5 nm), uniform, and amorphous-like carbon layer on the surface of NG particles. In the rate performances of coin-type cells with composite electrodes, an NG@C anode material delivers a high capacity of 348 mAh g^{-1} at a current rate of 5C,

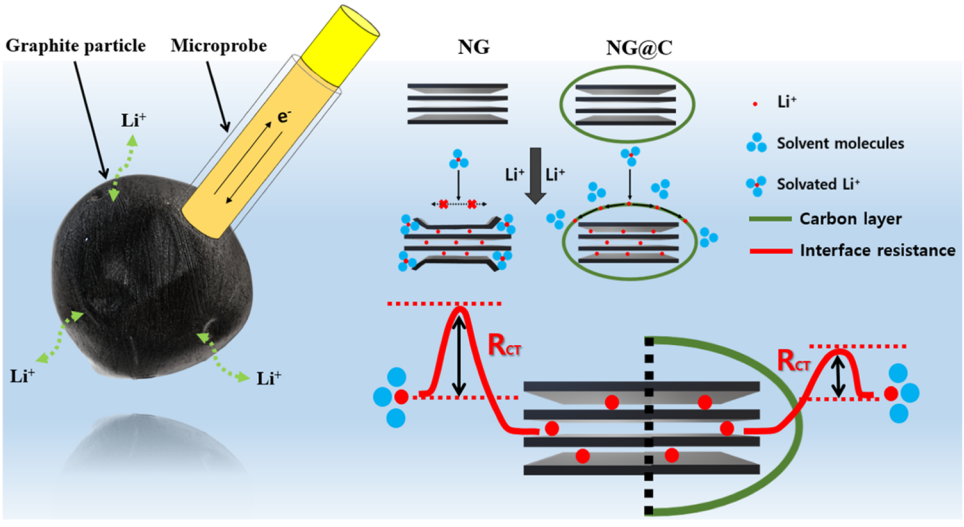

Figure 6. Illustration of a single-particle measurement and carbon layer protecting graphite to improve its kinetic parameters.

https://doi.org/10.1021/acsomega.3c08681
ACS Omega 2024, 9, 4004−4012

whereas pristine NG demonstrates only a capacity of 230 mAh g^{-1}. Moreover, the cycling test results at high current rates of 5C indicate that the NG and NG@C anode electrodes deliver maximum specific capacities of 179.2 and 339.4 mAh g^{-1} with their corresponding capacity retentions of 50 and 96% after 100 cycles, respectively. The results suggest that the coated carbon provides stability, desirable rate capability, and faster kinetics. To understand the influence of coated carbon on the interfacial kinetics, both NG and NG@C particles were studied by single-particle measurements. The interfacial charge transfer resistances of pristine and carbon-coated graphite were in the ranges of 81−101 and 49−67 Ω cm^2, respectively. The coated amorphous-like carbon reduces interfacial resistance and increases the exchange current density of graphite accordingly. The values might be varied depending on the type of carbonaceous material and/or carbon source for coating; however, the results suggest the importance of interface optimization for the high-power LIBs.

■ ASSOCIATED CONTENT

Supporting Information

The Supporting Information is available free of charge at https://pubs.acs.org/doi/10.1021/acsomega.3c08681.

Summary and after cycling results of Raman spectra, XPS survey, O 1s XPS spectra results, BET isotherms and BJH pore size distributions, voltage profiles at various current rates, EIS results, and XRD patterns at the initial stage and after 100 cycles in the 002 peak area (PDF)

■ AUTHOR INFORMATION

Corresponding Author

Sung-Soo Kim − *Graduate School of Energy Science and Technology, Chungnam National University, Daejeon 34134, Republic of Korea;* orcid.org/0000-0001-8969-7075; Email: kimss@cnu.ac.kr

Authors

Orynbassar Mukhan − *Graduate School of Energy Science and Technology, Chungnam National University, Daejeon 34134, Republic of Korea*

Ji-Su Yun − *Graduate School of Energy Science and Technology, Chungnam National University, Daejeon 34134, Republic of Korea*

Hirokazu Munakata − *Department of Applied Chemistry, Graduate School of Urban Environmental Science, Tokyo Metropolitan University, Tokyo 192-0397, Japan*

Kiyoshi Kanamura − *Department of Applied Chemistry, Graduate School of Urban Environmental Science, Tokyo Metropolitan University, Tokyo 192-0397, Japan*

Complete contact information is available at: https://pubs.acs.org/10.1021/acsomega.3c08681

Notes

The authors declare no competing financial interest.

■ ACKNOWLEDGMENTS

This work was supported by the Korea Institute of Energy Technology Evaluation and Planning (KETEP) funded by the Ministry of Trade, Industry & Energy (MOTIE) of the Republic of Korea (Grant Nos. 20011928 and 20016022).

■ REFERENCES

(1) Goodenough, J. B.; Park, K. S. The Li-Ion Rechargeable Battery: A Perspective. *J. Am. Chem. Soc.* **2013**, *135* (4), 1167−1176.

(2) Kulkarni, S.; Huang, T.-Y.; Thapaliya, B. P.; Luo, H.; Dai, Sh.; Zhao, F. Prospective Life Cycle Assessment of Synthetic Graphite Manufactured via Electrochemical Graphitization. *ACS Sustainable Chem. Eng.* **2022**, *10* (41), 13607−13618.

(3) Marom, R.; Amalraj, S. F.; Leifer, N.; Jacob, D.; Aurbach, D. A review of advanced and practical lithium battery materials. *J. Mater. Chem.* **2011**, *21*, 9938−9954.

(4) Kucinskis, G.; Bajars, G.; Kleperis, J. Graphene in lithium-ion battery cathode materials: A review. *J. Power Sources* **2013**, *240*, 66−79.

(5) Guoping, W.; Bolan, Z.; Min, Y.; Xiaoluo, X.; Meizheng, Q.; Zuolong, Y. A modified graphite anode with high initial efficiency and excellent cycle life expectation. *Solid State Ionics* **2005**, *176*, 905−909.

(6) Placke, T.; Siozios, V.; Schmitz, R.; Lux, S. F.; Bieker, P.; Colle, C.; Meyer, H. W.; Passerini, S.; Winter, M. Influence of graphite surface modifications on the ratio of basal plane to "non-basal plane" surface area and on the anode performance in lithium-ion batteries. *J. Power Sources* **2012**, *200*, 83−91.

(7) Aurbach, D.; Markovsky, B.; Weissman, I.; Levi, E.; Ein-Eli, Y. On the correlation between surface chemistry and performance of graphite negative electrodes for Li-ion batteries. *Electrochim. Acta* **1999**, *45*, 67−86.

(8) Seo, J.; Hyun, S.; Moon, J.; Lee, J. Y.; Kim, C. High performance of a Polydopamine-Coated Graphite Anode with a Stable SEI Layer. *ACS Appl. Energy Mater.* **2022**, *5*, 5610−5616.

(9) Kim, D. S.; Chung, D. J.; Bae, J.; Jeong, G.; Kim, H. Surface modifications of graphite anode material with black TiO_{2-x} for fast chargeable lithium-ion battery. *Electrochim. Acta* **2017**, *258* (20), 336−342.

(10) Tanaka, U.; Sogabe, T.; Sakagoshi, H.; Ito, M.; Tojo, T. Anode property of boron-doped graphite materials for rechargeable lithium-ion batteries. *Carbon* **2001**, *39* (6), 931−936.

(11) Lee, Y.; Jeghan, S. M. N.; Lee, G. Boost charging lithium-ion battery using expanded graphite anode with enhanced performance. *Mater. Lett.* **2021**, *299* (15), No. 130077.

(12) Wang, K.-X.; Li, X.-H.; Chen, J.-S. Surface and Interface Engineering of Electrode Materials for Lithium-Ion Batteries. *Adv. Mater.* **2015**, *27*, 527−545.

(13) Fu, L. J.; Liu, H.; Li, C.; Wu, Y. P.; Rahm, E.; Holze, R.; Wu, H. Q. Surface Modifications of Electrode Materials for Lithium Ion Batteries. *Solid State Sci.* **2006**, *8*, 113−128.

(14) Yamada, Y.; Noda, Y.; Munakata, H.; Yoshida, S.; Shibata, D.; Kanamura, K. Investigation of Carbon-coating Effect on the Electrochemical Performance of LiCoPO4 Single Particle. *Electrochemistry* **2018**, *85* (3), 145−151, DOI: 10.1149/MA2015-01/2/575.

(15) Kim, K.; Choi, H.; Kim, H.-J. Effect of carbon coating on nano-Si embedded SiO_x-Al_2O_3 composites as lithium storage materials. *Appl. Surf. Sci.* **2017**, *416*, 527−535.

(16) Kamiyama, A.; Kubota, K.; Nakano, T.; Fujimura, S.; Shiraishi, S.; Tsukada, H.; Komaba, S. High-Capacity Hard Carbon Synthesized from Macroporous Phenolic resin for Sodium-Ion and Potassium-Ion Battery. *ACS Appl. Energy Mater.* **2020**, *3*, 135−140.

(17) Mukhan, O.; Umirov, N.; Lee, B. M.; Yun, J. S.; Choi, J. H.; Kim, S. S. A Facile Carbon Coating on Mg-Embedded SiO_x Alloy for Fabrication of High-Energy Lithium-Ion Batteries. *Adv. Mater. Interfaces* **2022**, *9*, No. 2201426.

(18) Luo, W.; Wang, Y.; Chou, S.; Xu, Y.; Li, W.; Kong, B.; Dou, S. X.; Liu, H. K.; Yang, J. Critical thickness of phenolic resin-based carbon interfacial layer for improving long cycling stability of silicon nanoparticle anodes. *Nano Energy* **2016**, *27*, 255−264.

(19) Stephenson, D. E.; Hartman, E. M.; Harb, J. N.; Wheeler, D. R. Modeling of Particle-Particle Interactions in Porous Cathodes for Lithium-Ion Batteries. *J. Electrochem. Soc.* **2007**, *154*, A1146−A1155.

(20) Newman, J.; Thomas-Alyea, K. E. *Electrochemical Systems*, 3rd ed.; John Wiley & Sons Inc.: Hoboken, NJ, 2004.

(21) Suzuki, K.; Barbiellini, B.; Orikasa, Y.; Kaprzyk, S.; Itou, M.; Yamamoto, K.; Wang, Y. J.; Hafiz, H.; Uchimoto, Y.; Bansil, A.; Sakurai, Y.; Sakurai, H. Non-destructive measurement of in-operando lithium concentration in batteries via x-ray Compton scattering. *J. Appl. Phys.* **2016**, *119*, No. 025103.
(22) Heubner, C.; Langklotz, U.; Lammel, C.; Schneider, M.; Michaelis, A. Electrochemical single-particle measurements of electrode materials for Li-ion batteries: Possibilities, insights and implications for future development. *Electrochim. Acta* **2020**, *330*, No. 135160.
(23) Dokko, K.; Nakata, N.; Suzuki, Y.; Kanamura, K. High-Rate Lithium Deintercalation from Lithiated Graphite Single-Particle Electrode. *J. Phys. Chem. C* **2010**, *114*, 8646−8650.
(24) Lim, S.; Kim, J.-H.; Yamada, Y.; Munakata, H.; Lee, Y.-S.; Kim, S.-S.; Kanamura, K. Improvement of rate capability by graphite foam anode for Li secondary batteries. *J. Power Sources* **2017**, *355*, 164−170.
(25) Chae, J. E.; Annaka, K.; Hong, K.; Lee, S.-I.; Munakata, H.; Kim, S. S.; Kanamura, K. Electrochemical Characterization of Phosphorous-doped Carbon using Single Particle for Lithium Battery Anode. *Electrochim. Acta* **2014**, *130*, 60−65.
(26) Dokko, K.; Nakata, N.; Kanamura, K. High rate discharge capability of single particle electrode of $LiCoO_2$. *J. Power Sources* **2009**, *189*, 783−785.
(27) Lin, J.-H.; Chen, C.-Y. Thickness-controllable coating on graphite surface as anode materials using glucose-based suspending solutions for lithium-ion battery. *Surf. Coat. Technol.* **2022**, *436*, No. 128270.
(28) Sadezky, A.; Muckenhuber, H.; Grothe, H.; Niessner, R.; Pöschl, U. Raman microspectroscopy of soot and related carbonaceous materials: Spectral analysis and structural information. *Carbon* **2005**, *43* (8), 1731−1742.
(29) Blyth, R. I. R.; Buqa, H.; Netzer, F. P.; Ramsey, M. G.; Besenhard, J. O.; Golob, P.; Winter, M. XPS studies of graphite electrode materials for lithium ion batteries. *Appl. Surf. Sci.* **2000**, *167*, 99−106.
(30) Leofanti, G.; Padovan, M.; Tozzola, G.; Venturelli, B. Surface area and pore texture of catalysts. *Catal. Today* **1998**, *41*, 207−219.
(31) Wang, H.-L.; Shi, Z.-Q.; Jin, J.; Chong, C.-B.; Wang, C.-Y. Properties and sodium insertion behavior of Phenolic resin-based hard carbon microspheres obtained by a hydrothermal method. *J. Electroanal. Chem.* **2015**, *755*, 87−91.
(32) Gnanaraj, J. S.; Thompson, R. W.; Iaconatti, S. N.; DiCarlo, J. F.; Abraham, K. M. Formation and growth of surface films on graphitic anode materials for Li-ion batteries. *Electrochem. Solid-State Lett.* **2005**, *8* (2), A128−A132.
(33) Funabiki, A.; lnaba, M.; Ogumi, Z.; et al. Impedance study on the electrochemical lithium intercalation into natural graphite powder. *J. Electrochem. Soc.* **1998**, *145*, 172.
(34) Maher, K.; Yazami, R. A study of lithium ion batteries cycle aging by thermodynamics technique. *J. Power Sources* **2014**, *247*, 527−533.
(35) Ingole, R. S.; Rajagopal, R.; Mukhan, O.; Kim, S. S.; Ryu, K.-S. $LiNi_{0.6}Co_{0.2}Mn_{0.2}O2$ Cathode-Solid Electrolyte Interfacial Behavior Characterization Using Novel Method Adopting Microcavity Electrode. *Molecules* **2023**, *28*, 3537.
(36) Bard, A. J.; Faulkner, L. R. *Electrochemical Methods; Fundamentals and Applications*; John Wiley & Sons: New York, 1980; pp 87−106.
(37) Umeda, M.; Dokko, K.; Fujita, Y.; Mohammedi, M.; Uchida, I.; Selman, J. R. Electrochemical impedance study of Li-ion insertion into mesocarbon microbead single particle electrode: Part I. Graphitized carbon. *Electochim. Acta* **2001**, *14*, 885−890, DOI: 10.1016/S0013-4686(01)00799-X.
(38) Dokko, K.; Fujita, Y.; Mohammedi, M.; Umeda, M.; Selman, J. R. Electrochemical impedance study of Li-ion insertion into mesocarbon microbead single particle electrode: Part II. Disordered Carbon. *Electochim. Acta* **2001**, *47*, 933−938, DOI: 10.1016/S0013-4686(01)00809-X.
(39) Yoshio, M.; Wang, H.; Fukuda, K. Spherical Carbon-Coated Natural Graphite as a Lithium-Ion Battery-Anode Material. *Angew. Chem., Int. Ed.* **2003**, *42*, 4203−4206.

https://doi.org/10.1021/acsomega.3c08681
ACS Omega 2024, 9, 4004−4012